Available online at www.sciencedirect.com
ScienceDirect
Journal of the European Ceramic Society 31 (2011) 111–119
www.elsevier.com/locate/jeurceramsoc

Al_2O_3–SiC composites prepared by infiltration of pre-sintered alumina with a poly(allyl)carbosilane

Dušan Galusek [a,*], Róbert Klement [a], Jaroslav Sedláček [a], Miroslav Balog [b], Claudia Fasel [c], J. Zhang [b], M.A. Crimp [b], Ralf Riedel [c]

[a] *Vitrum Laugaricio – Joint Glass Centre of the Institute of Inorganic Chemistry, Slovak Academy of Sciences, Alexander Dubček University of Trenčín, Faculty of Chemical Technology STU, and RONA, j.s.c., Trenčín, Slovak Republic*
[b] *Department of Chemical Engineering and Materials Science, Michigan State University, East Lansing, USA*
[c] *Institute of Materials Science, Technische Universität Darmstadt, Darmstadt, Germany*

Received 8 April 2010; received in revised form 9 September 2010; accepted 14 September 2010

Abstract

The Al_2O_3/SiC nanocomposites containing 3–8 vol.% SiC were prepared through infiltration and *in situ* thermal decomposition of a preceramic polymer SiC precursor (poly(allyl)carbosilane) in pre-sintered alumina matrix. The volume fraction of SiC, and the microstructure of composites were adjusted by concentration of the polymer solution, and by the conditions of pyrolysis and sintering. The specimens were densified by pressureless sintering at temperatures between 1550 and 1850 °C in flowing argon. The use of powder bed producing SiO, CO and other volatile species suppressed decomposition reactions in the composites and was vital for their successful densification. The experimental results are discussed against thermodynamic analysis of the system Al_2O_3/SiC/SiO_2 in an inert Ar atmosphere.

Keywords: Nanocomposites; Al_2O_3; SiC; SiO_2; Sintering

1. Introduction

Addition of silicon carbide particles (SiC_p) or whiskers (SiC_w) has been reported to enhance strength,[1–6] fracture toughness,[1,6–8] wear resistance,[9–11] and creep resistance[12–14] of polycrystalline alumina. However, wider commercial utilization of the composites is limited due to lack of a cheap and reliable way of preparation of dense, defect-free ceramic bodies with complex shape containing homogeneously distributed SiC inclusions.

Standard processing procedure comprises wet mixing of alumina and SiC powders, drying, compacting, and high temperature densification. However, with submicrometre powders, it is difficult to prevent agglomeration and to ensure homogeneous mixing of SiC and Al_2O_3. Drying of suspensions is often an additional source of agglomeration, which results in uneven sintering, as well as void and crack formation during the high temperature densification. Moreover, pressureless sintering is problematic, most notably because the SiC inclusions inhibit densification by grain boundary pinning. Pressure-assisted techniques are therefore routinely applied, limiting the possibilities for production of more complex shapes and increasing the production costs. Alternative routes of preparation of the Al_2O_3–SiC composites are therefore of profound interest.

One of the promising methods utilizes organosilicon precursors, e.g. polycarbosilanes,[15–18] which can be converted into SiC through pyrolysis in inert atmosphere (Ar). The particles of alumina powder are usually coated with dissolved polymer, dried, cross-linked, compacted, pyrolysed and densified. Alternatively, the polymer-coated powder can be compacted by axial pressing at elevated temperature, condensing shaping and cross-linking into one processing step.[19] The precursor method allows formation of alumina-based nanocomposites with ultrafine particles of SiC (~12 nm) located either intra-[15,16] or inter-granularly,[17] which leads to enhanced mechanical strength.[20] Commercial availability of polymers that convert to β-SiC without excess carbon, which is known to impair mechanical properties,[21] opens new possibilities for preparation of SiC-reinforced composites.

* Corresponding author.
E-mail address: galusek@tnuni.sk (D. Galusek).

0955-2219/$ – see front matter © 2010 Elsevier Ltd. All rights reserved.
doi:10.1016/j.jeurceramsoc.2010.09.013

Chemical reactions that take place in the system in the course of high temperature densification represent a different problem. Due to the reactions, weight loss is often observed during sintering of SiC–Al_2O_3 compositions, mainly due to formation of CO, SiO, Al_2O and other gaseous species. Two main reactions occurring in different temperature intervals have been proposed to explain the weight loss.[22] At temperatures lower than 1600 °C, it is generally accepted that SiC reacts with a surface SiO_2 layer to produce SiO and CO. Above 1850 °C the weight loss results from reaction of SiC with Al_2O_3, yielding CO, SiO, and Al_2O. To suppress weight loss during sintering, samples are typically sintered using a powder bed and an inert atmosphere.[23]

This work studies the preparation of Al_2O_3–SiC composites with the use of a commercially available liquid polycarbosilane, which transforms by heating in inert atmosphere directly to β-SiC with high ceramic yield and without excess carbon. The liquid polymer can be infiltrated into open pores of pre-sintered alumina matrix. The volume fraction of polymer-derived SiC and the size of SiC particles were adjusted by the concentration of the polymer, and by conditions of pyrolysis and densification. The obtained results are confronted with the results of thermodynamic calculations in the system Al_2O_3–SiC–SiO_2 under sintering conditions.

2. Experimental

Ultrafine and ultrapure α-alumina powder Taimicron TM DAR (Taimei Chemicals Co., Ltd., Japan) with an average particle size of 150 nm was pressed uniaxially in a steel die at 50 MPa and then isostatically at 500 MPa in order to prepare pellets with diameter of 10 mm and height of 6 mm. The alumina green bodies were then pre-sintered in air in an electric furnace (HTM Reetz GmbH., Berlin, Germany, model LORA 1800) for 1 h at 1150 °C, which are the conditions ensuring sufficient mechanical strength of the pellet and at the same time maintaining the open porosity at the required level. The density was measured by Archimedes method in water and the porosity and pore size distribution were determined using a MicroMeritics 9320 Poresizer (MicroMeritics, Norcross, GA).

Liquid polycarbosilane SPM10 (StarFire Systems, Watervliet, NY) was used as the infiltration agent. By heating in inert atmosphere (Ar) the polymer transforms to β-SiC with high ceramic yield (75–80 wt.%, depending on temperature). The polymer is liquid, soluble in aprotic solvents, and can be handled in ambient environment.

The behaviour of the polymer in contact with α-Al_2O_3 was examined by simultaneous thermal analysis (STA, Netzsch STA 429, Netzsch-Gerätebau GmbH, Selb, Germany), coupled with mass spectrometry (Balzers MID) in the temperature range 20–1500 °C using a mixture of alumina powder with 10 wt.% of the polymer pre-crosslinked for 60 min at 400 °C. The results were compared with the data acquired from thermal analysis of the plain polymer.

The pre-sintered alumina pellets were infiltrated with the polymer, either concentrated, or dissolved in an appropriate volume of water-free cyclohexane (Sigma Aldrich, Steinheim, Germany) in order to prepare composites with 3, 5, and 8 vol.% SiC. The infiltration with the polymer solutions was carried out in static Ar atmosphere in a sealed glass container in order to avoid extended exposure of the polymer to moisture and air, and to prevent evaporation of the cyclohexane. The infiltration with concentrated viscous polymer (viscosity 80–150 mN s m^{-2} at 20 °C) was carried out at reduced pressure (approx. 200 Pa) in order to facilitate its penetration into the alumina matrix. The infiltration time was 48 h, which exceeded the time required for penetration into the whole volume of the pellet. After infiltration the excess polymer was removed from the specimen surfaces by paper tissue, after which the specimens were weighed. The solvent was evaporated by evacuation of the sample for 2 h at room temperature.

The pellets were then pyrolysed for 1 or 2 h in flowing Ar in a quartz tube at 1200 °C, and subsequently placed in a high temperature electric furnace with graphite heating elements for sintering under Ar for 3, 5, or 8 h at various temperatures between 1550 and 1850 °C. The pellets were protected with a powder bed with the composition: α-Al_2O_3 50 wt.%, SiC 25 wt.% and C (soot) 25 wt.%. The density of sintered specimens was determined by Archimedes method in water.

Pyrolysed and sintered samples were characterized by X-ray diffraction (XRD) and energy dispersive X-ray spectroscopy (EDX) carried out in conjunction with scanning electron microscopy (SEM). XRD measurements were carried out using a STOE STADIP powder diffractometer (STOE & CIE GmbH, Darmstadt, Germany) with Cu K_α radiation and scanned through 2θ angles between 30° and 70°. The microstructures were examined by SEM (Zeiss, model EVO 40HV, Carl Zeiss SMT AG, Germany) on polished and chemically etched (5 min in concentrated H_3PO_4 at 230 °C) cross sections of sintered specimens. The microstructures and the grain boundaries were investigated in detail by transmission electron microscopy (TEM) using an in-column omega filtered JEOL 2200 FS TEM/STEM (accelerating voltage 200 kV), equipped with an FE Gun and Oxford Instruments EDX system. TEM samples were prepared by dimpling the SiC composites to 20 μm, then ion-milling to perforation. Chemical analyses were performed by energy dispersive spectra collected at 200 kV (approx. 0.5 nm electron beam spot size), and by EDS using SEM operated at 5 kV.

The residual amount of SiC present after pyrolysis and sintering was verified by measuring the content of carbon, (LECO C200 carbon content analyzer, LECO Corp., St. Joseph, MI), assuming a stoichiometric conversion of the polymer with no free carbon.

The FactSage® software package[24] was used for thermodynamic (TD) calculations: the partial pressure of the gas phase and phase formation in the system Al–Si–C–O–Ar were calculated; Ar was considered as an inert gas. The required thermodynamic data were taken from the FactSage® databases, as well as from the special data set for the Al–Si–C system based on the work of Gröbner.[25] All relevant phases were included in the calculations. For modelling of phases the fully optimized FToxide database, which reproduces available phase diagrams was used. The gaseous species were considered down to a pressure of 10^{-10} Pa. For the metallic melt the RKMP model (Redlich–Kister–Maggiano polynomial) from the special data

set for the Al–Si–C system was used.[25] The calculations were performed at a given temperature under isobaric conditions; the total pressure was taken to be 0.1 MPa.

3. Results and discussion

3.1. Precursor decomposition

The poly(allyl)carbosilane precursor decomposition and formation of SiC, including possible oxidation in the course of the polymer pyrolysis, are prerequisites for phase and thermal stability, and due to phase development influence also the microstructure of prepared composites. The STA coupled with IR and mass spectrometry provided the information on decomposition of the pure polymer as well as the polymer in intimate contact with alumina powder (Fig. 1).

The STA data of the pure polymer revealed gradual mass loss (up to 24% at 1200 °C), accompanied by two pronounced endothermic (E_1, 62–284 °C, and E_2, 381–492 °C) and two exothermic effects between 520–930 °C (E_3) and 1076–1500 °C (E_4). These were attributed to cross-linking reactions (E_1), to the loss of hydrogen, SiH_x, and hydrocarbon units (E_2), to the formation of three-dimensional amorphous SiC network (E_3), and to the crystallization of β-SiC accompanied by the loss of residual hydrogen at temperatures below 1200 °C (E_4).

The STA data of alumina powder coated with 10 wt.% of partly cross-linked polymer also showed weight decrease in four subsequent steps, with 2.3% overall mass loss corresponding to 24% mass loss of the polymer in the mixture. The thermal effects are less distinguished than in the case of the pure polymer. The DTA curve contains one broad endothermic band (60–400 °C) and two pronounced exothermic effects in temperature intervals 400–780 °C and 990–1500 °C. These correspond to data from the pure polymer, with the exception of the cross-linking peak (E_1), which was observed in the pure polymer, but is missing in the polymer-coated (and pre-cross-linked) powder. The MS data (Fig. 1) yields additional information for interpretation of the STA results. Approximately 0.4% weight loss at temperatures up to 400 °C was attributed to desorption of water from the surface of alumina particles, and was confirmed by the presence of H_2O fragments ($z = 17, 18$) detected by MS at $T > 55$ °C. This effect was closely followed, and partly overlapped, by further weight decrease (1.2%) in two steps between 400 and 480 °C and between 480 and 750 °C respectively, accompanied by an endothermic and exothermic effect at the DTA curve. These were attributed to further cross-linking and gradual formation of the three dimensional SiC network. The MS data (Fig. 1) confirmed outgassing of hydrogen ($z = 2$), and hydrocarbons with $z = 12$–16 (C_1 fragments), $z = 24$–28 (C_2 fragments), and $z = 36$–44 (C_3 fragments). The $z = 28$–32 units, attributed to the formation of SiH_x were also detected as the results of cleavage of the polymer backbone. The units may also contain traces of carbon monoxide as the result of pyrolytic cracking of hydrocarbons, and the reaction of precipitated carbon with water vapour (Eq. (1)):

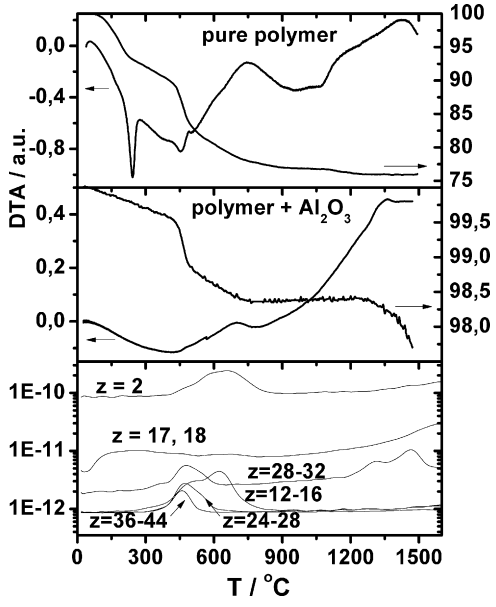

Fig. 1. The results of STA coupled with MS of the pure polymer and the polymer mixed with alumina powder.

$$C + H_2O \rightarrow CO + H_2 \quad (1)$$

Unlike the pure polymer, the TG of the coated powder shows no mass change in the temperature interval 750–1200 °C. Nevertheless, significant (0.6%) weight loss occurred above 1200 °C, which was not observed in the pure polymer, and was accompanied by the development of $z = 28$ units, which were identified as CO by IR-coupled MS. The CO formation was attributed to carbothermal reduction of silica, which, in some cases, is known to proceed at temperatures as low as 1300 °C.[26,27] The explanation is based on the presence and desorption of water from the surface of alumina powder particles at lower temperatures, resulting in partial hydrolysis of the polycarbosilane precursor, and formation of SiO_2. Silica reacts with traces of free carbon created by pyrolytic cracking of hydrocarbons, yielding SiC and CO (Eq. (2)):

$$SiO_2 + 3C \rightarrow SiC + 2CO \quad (2)$$

The results discussed in the two previous sections indicate that traces of water adsorbed at the surface of alumina powder particles may influence the phase composition of polymer derived alumina–SiC composites through partial hydrolysis and oxidation of the polymer precursor and formation of silica. In a positive case the silica eliminates the traces of free carbon from pyrolytic cracking of hydrocarbons, yielding SiC in the process. As a negative consequence, residual silica might alter the reactions taking place at higher temperatures, and, as shown by thermodynamic analysis, result in significant decomposition and loss of SiC from the composite.

3.2. Thermodynamic analysis of the system

The thermodynamic (TD) calculations were performed to simulate chemical reactions in the system Al_2O_3–SiC–SiO_2, containing 3, 5, and 8 vol.% of SiC, which corresponds to experimentally studied compositions. The 1 mol of reactants was used

in the calculations. The SiO_2 content in reaction simulations was set to 2 wt.% (1.344 mol%) with respect to SiC. For example, the amount of reactants used in the calculations for the sample with 8 vol.% of SiC is as follows: 0.8545 mol Al_2O_3, 0.1426 mol SiC, and 0.0019 mol SiO_2. To simulate the effect of the gas phase volume, the calculations were performed with 0.0001 mol, 0.001 mol, 0.01 mol, and 0.1 mol of Ar at the constant pressure of 10^5 Pa in the temperature range 1600–2200 °C. Various gas phase volumes have been considered, as due to the nature of high temperature experiment the determination of the exact amount of inert gas was not possible. The results thus provide a range of possible temperature intervals, which might be considered as a guideline for the experiment.

For better understanding of the reactions that take place in the studied system, simulations of thermochemical reactions in a SiC–SiO_2 system were also carried out, and the results (see supplementary materials) are very similar to those published by Cupid et al.[28] The two key reactions (Eqs. (3) and (4)) were identified to be responsible for the SiC decomposition; reaction (3) at lower temperatures and reaction (4) at higher temperatures, when all SiO_2 is consumed.

$$SiC(s) + 2SiO_2(s, l) = 3SiO(g) + CO(g) \quad (3)$$

$$SiC(s) + SiO(g) = 2Si(l) + CO(g) \quad (4)$$

The results of the calculations (the phase fraction diagrams) for the system Al_2O_3–SiC–SiO_2 with 8 vol.% of SiC are shown in Fig. 2. According to the calculations, all of the SiO_2 reacts with Al_2O_3, yielding mullite phase in equilibrium with excess Al_2O_3. Up to 1734 °C, the main gas species are SiO and CO in the molar ratio SiO/CO = 3. This indicates that the main reaction proceeds between SiC and SiO_2 from mullite, yielding Al_2O_3 and gas species:

$$3Al_2O_3{\cdot}2SiO_2(s) + SiC(s) = 3Al_2O_3(s) + 3SiO(g) + CO(g) \quad (5)$$

The mullite phase is completely consumed at 1862 °C (0.0001 mol Ar), 1840 °C (0.001 mol Ar), and 1735 °C (0.01 mol Ar), respectively. However, when 0.1 mol of Ar was used in the calculation, no mullite phase was found to be stable above 1600 °C. When all mullite is consumed, the phase equilibria proceed in a more complicated way and the reactions taking place in the system can be schematically described by Eqs. (4) and (6) as reported also by Can et al.[29] and Ihle et al.,[30] respectively:

$$4SiC(s) + 2Al_2O_3(s, l) = 4CO(g) + SiO(g) + Al_2O(g) + 3Si(l) + 2Al(l, g) \quad (6)$$

According to the calculations, all of the SiC in the system is consumed at 2050 °C (0.0001 and 0.001 mol Ar) or at 2046 °C (0.01 mol Ar). At this temperature the amount of the formed liquid metal solution (onset of formation at 1734 °C) reaches a maximum and starts to decrease with increasing temperature. The amount of the gas phase increases with temperature at approximately the same rate as the amount of liquid metal decreases. The increase of the amount of the gas phase is mainly the result of formation of SiO and Al_2O, while the contribution

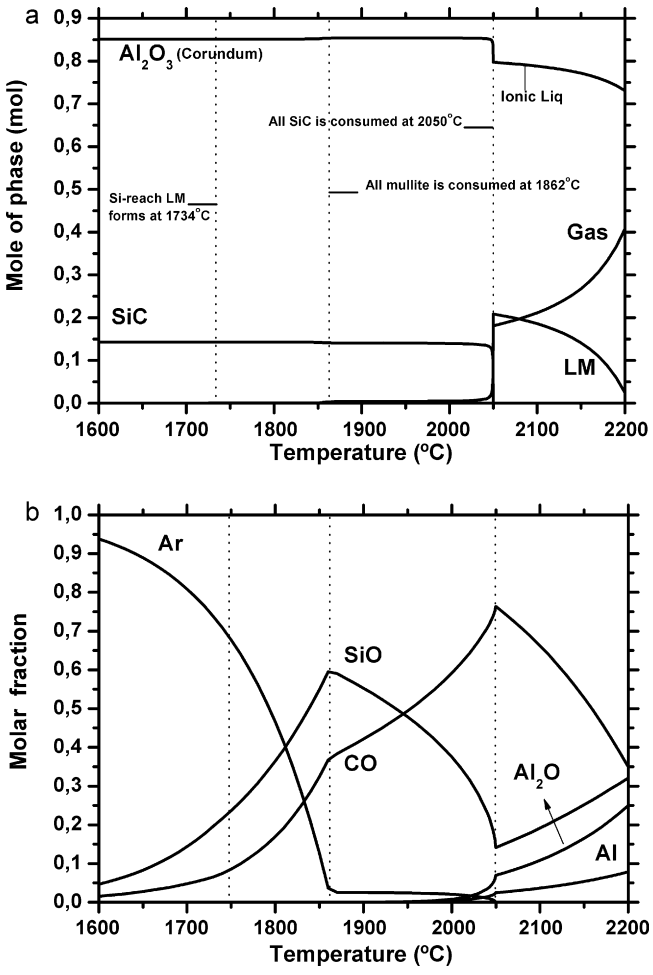

Fig. 2. Results of thermochemical reaction calculations for Al_2O_3 and SiC with 0.0001 mol of inert gas Ar (a) Phase fraction diagram. (b) Gas phase composition. Mullite is not shown due to its formation in a very small amount (~0.001 mol).

of CO formation is small. The slight increase in CO reflects the small amount of free carbon, which is dissolved in the Si–Al melt. The amount of ionic liquid (Al_2O_3) decreases (Fig. 2). This implies the reactions between Al_2O_3 and constituents of liquid metal solution (Si, Al and C) or element gas species Si(g) and Al(g). The reactions that may proceed in the system at higher temperatures (>2050 °C) can thus be schematically expressed as follows:

$$Al_2O_3(l) + 3C(s, sol) = 2Al(l, g) + 3CO(g) \quad (7)$$

$$Al_2O_3(l) + 4Al(l, g) = 3Al_2O(g) \quad (8)$$

$$Al_2O_3(l) + 2Si(l, g) = 2SiO(g) + Al_2O(g) \quad (9)$$

The reactions schemes for the vapourization of SiC–Al_2O_3 system at the excess of C, Si and Al have been proposed by Baud et al.[31] The reactions (8) and (9) between Al_2O_3 and either Si or Al at high temperatures were also proposed by other authors.[32,33] The calculations in systems containing 3 and 5 vol.% of SiC yielded similar results. When atmosphere produced by the powder bed (mixture of Al_2O_3, SiC and C), instead of Ar, was used in the calculation, formation of significant amount of gasses CO,

Table 1
Carbon content vs. the conditions of heat treatment.

Sample	Heat treatment	C [wt.%]	SiC [vol.%]
IP8-1	950 °C/60′	3.03 ± 0.04	12.6
IP8-2	1550 °C/60′	3.01 ± 0.08	12.5
IP8-3	1550 °C/180′	2.54 ± 0.26	10.6
IP8-4	1650 °C/180′	2.19 ± 0.13	9.1

SiO and Al_2O (predominantly CO) effectively suppress above described reactions.

The so called "nano-effect", that could significantly influence the thermodynamics of the systems due to high contribution of particles' surfaces, and even decrease the minimum temperature for some processes, is not included in the TD calculations presented in this paper. Nevertheless, the results indicate a profound influence of silica, usually present in the system as the product of low temperature oxidation of SiC, and of the amount of inert gas on thermal stability, phase composition, and decomposition reactions in the system Al_2O_3–SiC. These results are discussed in following sections with respect to experimental data.

3.3. Phase composition

The carbon content measurements (accounting also for carbon bound as SiC) showed a notable decrease in concentration with increased temperature and time of heat treatment. If all carbon is considered to be bound to silicon as SiC, the approximate fraction of SiC can be calculated at each respective temperature. The results are shown in Table 1. The amount of carbon decreased from the equivalent of 12.6 vol.% SiC at 950 °C, when the polymer-to-ceramic conversion was completed, to the equivalent of 9.1 vol.% SiC after 3 h treatment at 1650 °C. The decrease was attributed especially to chemical reactions described by the reaction equation (5), as the consequence of formation of mullite in the composite from silica created by partial hydrolysis and oxidation of polymer by water adsorbed on alumina powder. SiO and CO were the main gas products of decomposition of the composite. The CO and SiO-generating powder bed, consisting of Al_2O_3, SiC, and C (soot), was therefore applied in order to suppress the decomposition reactions at higher temperatures.

Fig. 3 summarises the XRD patterns of the plain SP-Matrix polymer heat treated for 3 h at 1550 °C, and of the specimens infiltrated with the equivalent of 8 vol.% SiC of the polymer (IP8), heat treated for 60 min at 1550 and 1700 °C, respectively. The plain polymer crystallized directly to β-SiC and significant peak broadening indicates a nanocrystalline nature of the crystalline product. The diffraction pattern of the IP8 after heat treatment at 1550 °C shows partial overlapping of the two most intensive β-SiC peaks (102 at $d = 2.516$ Å, $2\Theta = 35.65°$ and 110 at $d = 1.541$ Å, $2\Theta = 60.02°$) with the peaks of α-alumina at $d = 2.551$ Å ($2\Theta = 35.61°$), and 1.540 Å, respectively. However, a shoulder at $d = 2.52$ Å observed in the diffraction pattern of the IP8, and the intensity of the peak at $d = 1.541$ Å stronger than would correspond to the respective peak of α-Al_2O_3 indicate the presence of crystalline β-SiC in the sample. Neither mullite nor

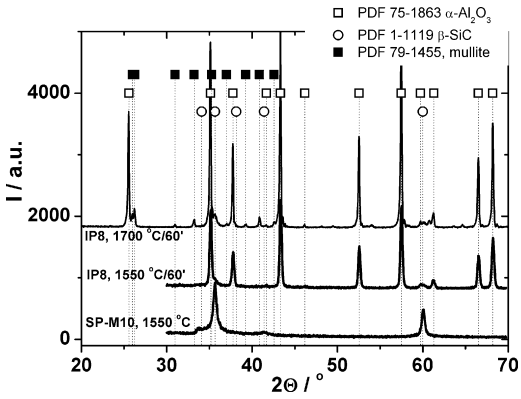

Fig. 3. Diffraction patterns of the SP-Matrix polymer and the IP8 sample after heat treatment at 1550 °C, and at 1700 °C.

any crystalline form of silica were detected. However, after heat treatment at 1700 °C, evidence of mullite formation was found, demonstrated especially by the presence of two diffraction peaks at 2Θ values 25.978° and 26.264°. This result is in accord with the results of TD analysis, which predicts formation of mullite in the system containing silica as the result of oxidation of the polymer precursor, and reaction of silica from mullite with SiC, yielding alumina, SiO and CO (Eq. (5)) up to a temperature of 1862 °C. In addition, the intensity of β-SiC diffraction peak at $2\Theta = 35.65°$ increases (from indistinct shoulder at 1550 °C to a well defined peak at 1700 °C), indicating enhanced crystallinity or crystallite size growth with increasing temperature.

3.4. Densification and microstructure

All specimens sintered at temperatures exceeding 1750 °C without the powder bed were decomposed, porous, and white in colour, which suggests complete loss of SiC as the result of reactions (5), and possibly, 3. Interestingly, complete loss of SiC was observed at lower temperatures than predicted by thermodynamic calculations, which is attributed to a flow-through atmosphere and removal of gaseous reaction products, not considered in the calculations. Efficient protection of the specimen and suppression of decomposition reactions was achieved by the use of the CO and SiO-producing powder bed, which shifted the reaction equilibrium towards the reactants.

The sintering between 1700 and 1850 °C with applied powder bed in all cases yielded composites with relative densities approaching or exceeding 90%. At lower sintering temperatures (1700 °C) the sintered density was strongly influenced by the volume fraction of SiC in the material: the composite with 3 vol.% of SiC (IP3) sintered to less than 5% of the residual porosity, while the materials with 5 and 8 vol.% of SiC (IP5 and IP8) were only about 90% dense. In the case of IP3, smaller silicon carbide particles were not sufficient to achieve any observable grain boundary pinning effect, and densification was not markedly impaired. This was, in turn, reflected in a coarser microstructure of IP3, resulting from a higher grain boundary mobility in the composite with low volume fraction and smaller number of small intergranular SiC inclusions. At temperatures ≥1750 °C no significant difference of relative

density was observed, irrespective of the SiC volume fraction in the material. The main difference was in the size of the alumina matrix grains, which increased with increasing temperature and decreasing volume fraction of SiC (Fig. 3). This indicates that the grain boundary diffusion responsible for densification, as well as grain boundary mobility responsible for matrix grain growth, was markedly influenced by the volume fraction of SiC. There are several mechanisms that can be considered. Firstly, silica segregation at alumina–alumina, and alumina–SiC grain boundaries, may markedly influence both the grain boundary diffusion and grain boundary mobility responsible for densification and grain growth, respectively. However, according to the results of the thermodynamic analysis and the X-ray diffraction, silica is bound in the form of mullite at relatively low temperatures, which is then completely consumed in the temperature interval between 1600 and 1862 °C, depending on the amount of inert gas applied during high temperature treatment. Although some formation of Si-rich metallic melt above 1734 °C is predicted by the calculations, these also predict only low amounts of such a phase at any temperature below 1850 °C. Clean, melt- or glass-free grain boundaries can be therefore expected under the conditions applied. These results are confirmed by TEM examination of the nanocomposites. A micrograph of the material containing 3 vol.% of SiC shows spherical SiC nanoparticles with diameters between 5 and 30 nm distributed within an alumina matrix grain is shown in Fig. 4a. A large single intragranular SiC particle with a diameter of 250 nm is shown in Fig. 4b: characteristic stacking faults are visible in the particle. The grain boundary between the particle and the alumina matrix grain appear to be clean and free of any amorphous phase. The result, which is in accord with the results of thermodynamic calculations mentioned above, is confirmed by the high resolution TEM micrograph showing a typical SiC–Al_2O_3 grain boundary with direct contact of crystalline SiC and Al_2O_3 phases.

The different densification rate is therefore most likely the consequence of the different number, and volume, of the intergranular SiC particles: higher volume fraction of SiC particles increases the total area of SiC–alumina grain boundaries on account of alumina–alumina boundaries, altering the energy requirements for grain boundary diffusion and grain boundary mobility. At 1700 °C the energy requirements for grain boundary diffusion are satisfied only for the composite IP3: composites with larger area fractions of alumina–SiC grain interfaces require more energy (higher temperature) for successful densification. At temperatures ≥1750 °C this condition could be regarded as satisfied for all SiC contents. Such high temperatures enhance the grain boundary mobility, and in specimens with higher SiC contents also promote the growth of SiC particles by coalescence, or possibly also by evaporation–condensation mechanism. At 3 vol.% of SiC the small SiC particles are engulfed by fast moving boundaries (Figs. 4a and 5a). In composites IP5 and IP8 the coalescence is so pronounced that grain boundaries are effectively pinned with numerous large SiC inclusions (Fig. 5b). Here, intergranular SiC particles with high aspect ratio are observed, and the materials sintered at 1850 °C contain numerous SiC whiskers situated parallel to the boundary. The breakaway of a particle with such geometry from the grain

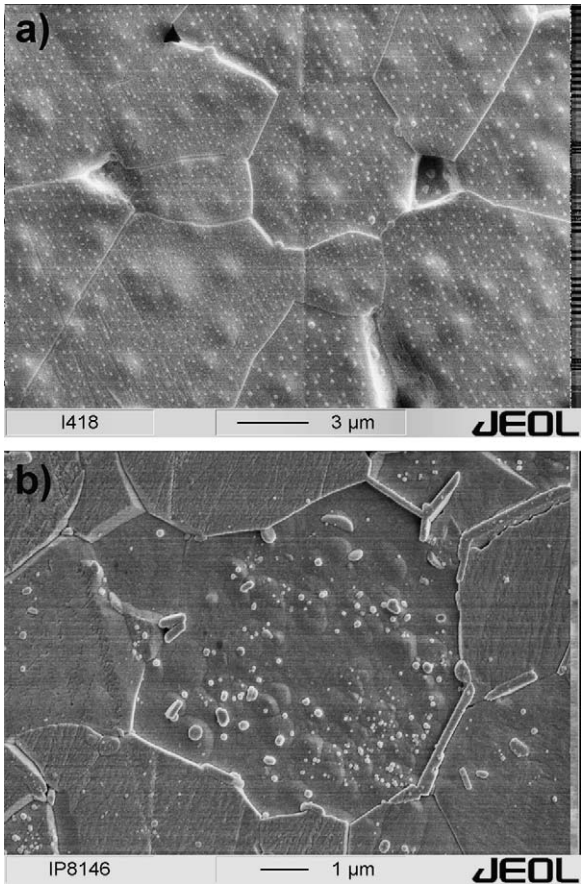

Fig. 4. SEM micrographs of Al_2O_3–SiC composites with 3 vol.% of SiC sintered for 3 h at 1800 °C (a), and with 8 vol.% of SiC sintered for 3 h at 1850 °C (b).

boundary is energetically so demanding that it can act as an effective pinning site. The presence of particles with elongated morphology also supports the hypothesis of the growth of SiC particles by evaporation–condensation mechanism. The TEM micrograph in Fig. 6a shows the typical microstructure of the nanocomposite containing 8 vol.% SiC sintered 3 h at 1850 °C. Along with SiC whiskers situated parallel to alumina–alumina grain boundaries, numerous spherical intragranular SiC particles with diameters between 25 and 120 nm are observed. Stacking faults are present both in the whiskers and in some of the spherical inclusions. In accordance with the results of the TD calculations, the interfaces between the two intragranular spherical SiC inclusions and the embedding alumina matrix grain shown in Fig. 6b appear to be clean without any amorphous second phase. Some confusion is introduced by the EDX point analysis of selected places in the specimen, as shown in Fig. 6c. While in the whiskers (EDX spectra 2 and 3) the analysis identified Si and C, with some traces of Al likely originating from the surrounding alumina matrix, in the intragranular SiC inclusions the analysis revealed, along with expected Si and C, also the presence of Al and O (EDX spectra 4 and 6). However, a significant contribution to the EDX spectra is expected from the surrounding alumina matrix due to the small dimensions of intragranular particles in comparison to whiskers, which may explain the high intensity of aluminium and oxygen peaks. The only exception is analysis

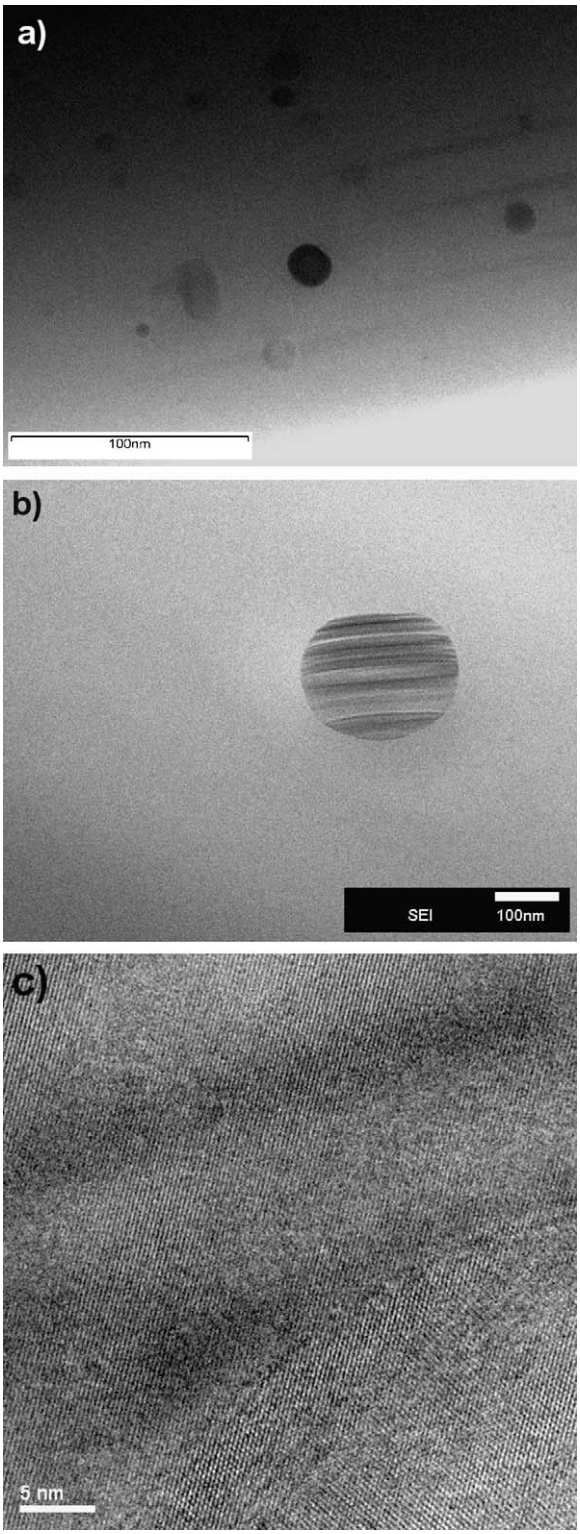

Fig. 5. The results of TEM examination of the Al_2O_3–SiC composite with 3 vol.% of SiC sintered for 3 h at 1800 °C: overall view (a), secondary electron image of a single SiC particle embedded within the alumina matrix (b), and a HRTEM image showing the Al_2O_3/SiC grain boundary (c).

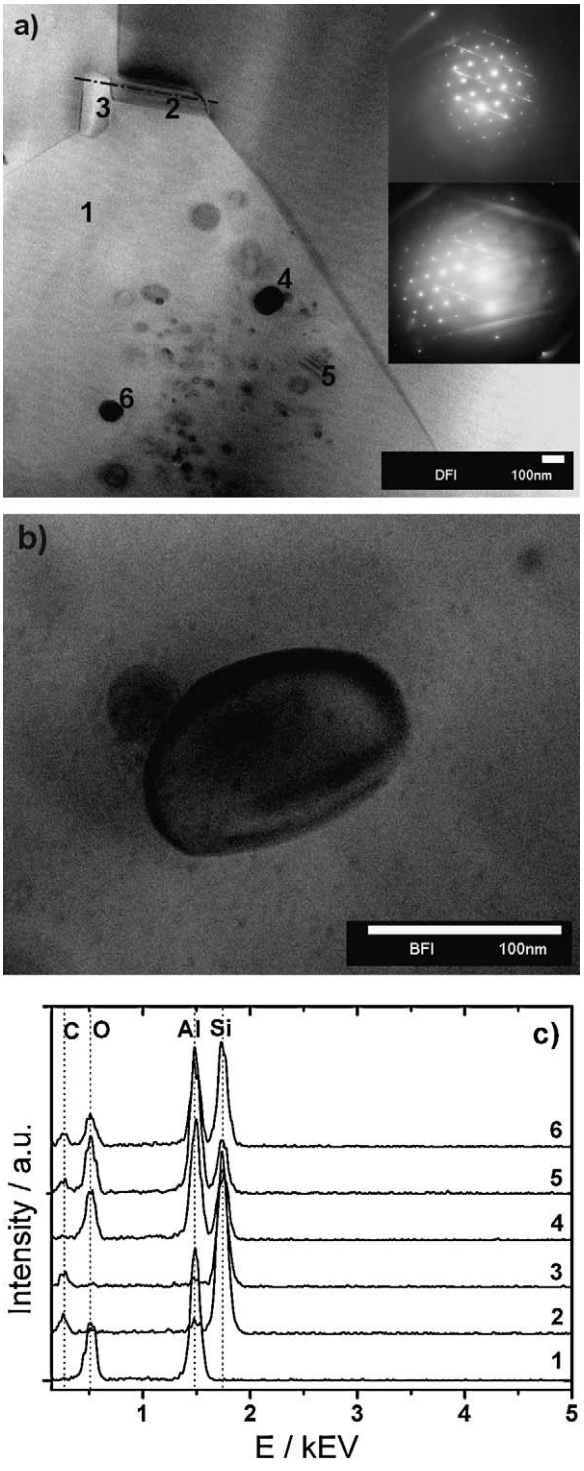

Fig. 6. The results of TEM examination of the Al_2O_3–SiC composite with 8 vol.% of SiC sintered for 3 h at 1850 °C: overall view (a), higher magnification micrograph of an intragranular SiC nanoparticle (b), EDX point analyses of numbered places in the image (c). Upper and lower insets show the respective electron diffraction patterns from points 2 and 5.

No. 4, where Al, Si, and O, but no carbon, was detected, and the analysis can be interpreted as a detection of a mullite inclusion. Despite the fact that the thermodynamic analysis predicts disappearance of mullite between 1600 and 1862 °C depending on the amount of inert gas applied during high temperature treatment, its retention can be explained as follows: mullite decomposes through its reaction with SiC (Eq. (5)). However, if a mullite grain is embedded within an alumina matrix grain at a relatively low temperature (e.g. 1500 °C), its reaction counterpart

is missing and the reaction cannot proceed. Some presence of mullite can be therefore expected in all Al_2O_3–SiC nanocomposites prepared from SiO_2-contaminated SiC powder, or from a partly oxidised or hydrolysed preceramic polymer precursor of SiC.

4. Conclusions

The paper summarises the experimental data obtained for the nanocomposites prepared through *in situ* thermal decomposition of the SiC preceramic polymer in alumina matrix with subsequent pressureless sintering in Ar atmosphere, discussed against the results of thermodynamic analysis of the system Al_2O_3/SiC/SiO_2.

The results can be summarised as follows:

1. The pre-ceramic polymer in direct contact with moisture-contaminated submicron alumina powder reacted with H_2O vapour, yielding an oxygen containing polymer, which finally led to the formation of SiO_2 or mullite during further heating at $T < 1550\,^{\circ}C$.
2. The TD analysis predicted a profound influence of the silica contamination and the amount of inert gas in the system on the temperature of formation and disappearance of various phases, including mullite or Si-rich metallic melt, and on the final phase composition of the composite.
3. In the absence of the CO and SiO-producing protective powder bed, the presence of silica and mullite in the material led to the decomposition and complete loss of SiC at $T > 1750\,^{\circ}C$.
4. The use of the protective powder bed facilitated the preparation of nearly fully dense Al_2O_3/SiC nanocomposites with SiC content between 3 and 8 vol.% by pressureless sintering between 1750 and 1850 °C.
5. The TEM examination of the prepared nanocomposites confirmed, in accord with the TD analysis, the absence of any intergranular glass at Al_2O_3/SiC grain boundaries. However, the EDX analysis gave some evidence on the retention of discrete mullite particles in materials sintered at temperatures as high as 1850 °C.

Acknowledgements

This publication was created in the frame of the project "Centre of excellence for ceramics, glass, and silicate materials" ITMS code 262 201 20056 based on the Operational Program Research and Development funded from the European Fund of Regional Development. The financial support of this work by the Alexander von Humboldt Foundation, Bonn, Germany (D. Galusek and R. Riedel), by the APVV grant No 0485-06, by the grant APVV LPP 0297-09, and by the J. Fulbright Commission in the Slovak Republic (M. Balog) is also gratefully acknowledged. The JEOL 2200 FX used in this study was purchased using funds from the US National Science Foundation. The authors are also grateful to the Starfire Systems, Malta, NY, for providing the SPM-10 polymer used in this study.

Appendix A. Supplementary data

Supplementary data associated with this article can be found, in the online version, at doi:10.1016/j.jeurceramsoc.2010.09.013.

References

1. Niihara K. New design concept of structural ceramics—ceramic nanocomposites. *J Ceram Soc Jpn* 1991;**99**:974–82.
2. Davidge RW, Brook RJ, Cambier F, Poorteman M, Leriche A, O'Sullivan D, et al. Fabrication, properties, and modelling of engineering ceramics reinforced with nanoparticles of silicon carbide. *Br Ceram Trans* 1997;**96**:121–7.
3. Perez-Rigueiro J, Pastor JY, Llorca J, Elices M, Miranzo P, Moya JS. Revisiting the mechanical behaviour of alumina silicon carbide nanocomposites. *Acta Mater* 1998;**46**:5399–411.
4. Wu HZ, Lawrence CW, Roberts SG, Derby B. The strength of Al_2O_3/SiC nanocomposites after grinding and annealing. *Acta Mater* 1998;**46**:3839–48.
5. Zhao J, Stearns LC, Harmer MP, Chan HM, Miller GA. Mechanical behaviour of alumina silicon-carbide nanocomposites. *J Am Ceram Soc* 1993;**76**:503–10.
6. Jiang DL, Huang ZR. SiC whiskers and particles reinforced Al_2O_3 matrix composites and N_2-HIP post-treatment. *Key Eng Mater* 1999;**159–160**:379–86.
7. Collin MIK, Rowcliffe DJ. Influence of thermal conductivity and fracture toughness on the thermal shock resistance of alumina-silicon-carbide-whisker composites. *J Am Ceram Soc* 2001;**84**:1334–40.
8. Akatsu T, Suzuki M, Tanabe Y, Yasuda E. Effects of whisker content and dimensions on the R-curve behaviour of an alumina matrix composite reinforced with silicon carbide whiskers. *J Mater Res* 2001;**16**:1919–27.
9. Davidge RW, Twigg PC, Riley FL. Effects of silicon carbide nano-phase on the wet erosive wear of polycrystalline alumina. *J Eur Ceram Soc* 1996;**16**:799–802.
10. Sternitzke M, Dupas E, Twigg PC, Derby B. Surface mechanical properties of alumina matrix nanocomposites. *Acta Mater* 1997;**45**:3963–73.
11. Chen HJ, Rainforth WN, Lee WE. The wear behaviour of Al_2O_3–SiC ceramic nanocomposites. *Scripta Mater* 2000;**42**:555–60.
12. De Arellano-Lopez AR, Dominguez-Rodriguez A, Routbort L. Microstructural constraints for creep in SiC-whisker-reinforced Al_2O_3. *Acta Mater* 1998;**46**:6361–73.
13. Deng Z-Y, Shi J-L, Zhang Y-F, Lai T-R, Guo J-K. Creep and creep-recovery behaviour in silicon-carbide-particle-reinforced alumina. *J Am Ceram Soc* 1999;**82**:944–52.
14. Tai Q, Mocellin A. Review: high temperature deformation of Al_2O_3-based ceramic particle or whisker composites. *Ceram Int* 1999;**25**:395–408.
15. Su B, Sternitzke M. In: Bellosi A, editor. *IV Euro Ceramics, vol. 4, Basic Science and Trends in Emerging Materials and Applications*. Italy: Grupp Editoriale Faenza Editrice S.p.A.; 1995. p. 109–16.
16. Sternitzke M, Derby B, Brook RJ. Alumina/silicon carbide nanocomposites by hybrid polymer/powder processing: microstructures and mechanical properties. *J Am Ceram Soc* 1998;**81**:41–8.
17. Sawai Y, Yasutomi Y. Effect of high-yield polycarbosilane addition on microstructure and mechanical properties of alumina. *J Ceram Soc Jpn* 1999;**107**:1146–50.
18. Narisawa M, Okabe Y, Okamura K, Kurachi Y. Synthesis of nano size dispersed silicon carbide particles by firing inorganic–organic hybrid precursors. *Key Eng Mater* 1999;**159–160**:101–6.
19. Galusek D, Sedláček J, Riedel R. Al_2O_3–SiC composites by warm pressing and sintering of an organosilicon polymer-coated alumina powder. *J Eur Ceram Soc* 2007;**27**:2385–92.
20. Galusek D, Sedláček J, Švančárek P, Riedel R, Satet R, Hoffmann M. The influence of post-sintering HIP on the microstructure, hardness, and indentation fracture toughness of polymer-derived Al_2O_3–SiC nanocomposites. *J Eur Ceram Soc* 2007;**27**(2–3):1237–45.

21. Bill J, Aldinger F. Precursor-derived covalent ceramics. *Adv Mater* 1995;**7**:775–87.
22. Grande T, Sommerset H, Hagen E, Wiik K, Eiinarsrud M-A. Effect of weight loss on liquid-phase-sintered silicon carbide. *J Am Ceram Soc* 1997;**80**:1047–52.
23. Winn EJ, Clegg WJ. Role of the powder bed in the densification of silicon carbide sintered with yttria and alumina additives. *J Am Ceram Soc* 1999;**82**:3466–70.
24. Bale CW, Chartrand P, Degterov SA, Eriksson G, Hack K, Ben Mahfoud R, et al. FactSage thermochemical software and databases. *Calphad* 2002;**26**:189–228.
25. Gröbner J, Lukas HL, Adlinger F. Thermodynamic calculation of the ternary system Al–Si–C. *Calphad* 1996;**20**:247–54.
26. Kevorkijan VM, Krizman A. Carbothermal synthesis of submicrometer β-SiC powder using double precursor reaction mixture. *Ceram Trans* 1995;**51**:127–31.
27. Cheng Z, Sacks MD, Wang CA. Synthesis of nanocrystalline silicon carbide powders. *Ceram Eng Sci Proc* 2003;**24**:23–32.
28. Cupid DM, Fabrichnaya O, Seifert HJ. Thermodynamic aspects of liquid phase sintering of SiC using Al_2O_3 and Y_2O_3. *Int J Mater Res* 2007;**25**:976–86.
29. Can A, Hermann M, McLachlan DS, Sigalas I, Adler J. Densification of liquid phase sintered silicon carbide. *J Eur Ceram Soc* 2006;**26**:1707–13.
30. Ihle J, Hermann M, Adler J. Phase formation in porous liquid phase sintered silicon carbide. Part III. Interaction between Al_2O_3–Y_2O_3 and SiC. *J Eur Ceram Soc* 2005;**25**:1005–113.
31. Baud S, Trévenot F, Chatillon C. High temperature sintering of SiC with oxide additives. III. Quantitative vaporization of SiC–Al_2O_3 powder beds as revealed by mass spectrometry. *J Eur Ceram Soc* 2003;**23**:19–27.
32. Gao KY, Speck F, Emtsev K, Seyller Th, Ley L. Thermal stability of surface and interface structure of atomic layer deposited Al_2O_3 on H-terminated silicon. *J Appl Phys* 2007;**102**:094503.
33. Fujii H, Umakoshi H, Aoki Y, Nogi K. Bubble formation in aluminium alloy during electron beam welding. *J Mater Process Technol* 2004;**155–156**:1252–5.